Kinetics and Mechanism of the Reversible Dissociation of Ammonium Carbamate: Involvement of Carbamic Acid

B. R. Ramachandran, Arthur M. Halpern,* and Eric D. Glendening

Department of Chemistry, Indiana State University, Terre Haute, Indiana 47809

Received: December 2, 1997; In Final Form: March 26, 1998

The kinetics of the reversible decomposition of ammonium carbamate, $NH_4CO_2NH_2$ (AC), into NH_3 (A) and CO_2 (C) has been studied between 278 and 312 K by recording the time dependence of the total pressure above an AC sample that, after being previously evacuated, is exposed to the headspace of an isoteniscope. At early times (<1 s), the data show an inflection, which is enhanced in first derivative transformations. Three mechanisms are discussed, each containing six rate constants. Two assume the presence of gas phase carbamic acid (CA) as an intermediate. These mechanisms are explored further through ab initio computational studies of CA. These results indicate that gas phase CA is a very stable species. No evidence could be found for its presence from Fourier transform IR spectra of the equilibrium vapor above AC. The mechanism that we suggest involves the reversible decomposition of AC into surface-bound CA, A, and C molecules, with the latter two reversibly desorbing from the surface. The experimental kinetic data are consistent with all three mechanisms. The rate data do not contain sufficient information to allow all rate constants to be uniquely determined. Simulation studies are used to demonstrate consistency of the mechanisms with the data.

Introduction

Ammonium carbamate, $NH_4CO_2NH_2$ (AC), is a solid material that coexists with its decomposition products, the small molecules CO_2 (C) and NH_3 (A). This heterogeneous equilibrium arises from the reversible dissociation process

$$NH_4CO_2NH_2(s) \rightleftarrows 2NH_3(g) + CO_2(g) \qquad (1)$$

Above about 400 K, AC dissociates into water and urea.[1] At ambient temperature the equilibrium partial pressures of C and A are appreciable. For example, the equilibrium dissociation pressure, P_{eq}, above solid AC is 85 Torr at 298 K, and it reaches 1 atm at 332 K. Furthermore, as these data imply, the dissociation pressure of AC is strongly temperature dependent, with a temperature coefficient of about 12.8 kcal/mol, which is one-third of the enthalpy of reaction. The equilibrium properties of the AC system have been well characterized, and there are several reports in the literature concerning the temperature dependence of the vapor pressure of AC.[2−4]

Several attempts have been made to analyze the kinetics of the AC $\rightleftarrows$ 2A + C reactions. Laurent and Kikindai[1] studied the time dependence of the formation of solid AC from A and C and obtained rate constants for this process between 296 and 433 K (a range that also encompasses the complication of urea formation). In this study, Laurent and Kikindai[1] assumed an overall third-order process to account for the formation of solid AC (with partial orders of one and two with respect to A and C, respectively) and, furthermore, assumed a zero-order process for the reverse reaction decomposition. The results of this investigation are questionable because the temperature dependence of the equilibrium pressures reported by these workers does not agree with literature values and, furthermore, the validity of the termolecular elementary step was not substantiated.

Frejacques[5] assumed an empirical second-order rate expression, i.e., $a - bP^2$, for the decomposition of AC. Again, no mechanism was suggested to rationalize this rate law. Lishnevskii and Madzievskaya[6] studied the formation of solid AC between 195 and 293 K and its decomposition between 263 and 303 K, by measuring initial rates of reaction. They allude to a mechanistic scheme that involves the initial adsorption of NH_3 and CO_2 onto the surface of the solid and a subsequent surface reaction, leading to the formation of AC. They also invoked the intermediacy of carbamic acid, NH_2CO_2H (CA), on the surface. Their kinetic analysis, however, is limited only to the temperature dependence of the initial rates of the forward and back reactions. No rate equation pertaining to any mechanism was presented.

Claudel and Boulamri[7] studied the reaction kinetics in both the forward and reverse directions and fit the total pressure data to an empirical second-order polynomial represented by

$$dP/dt = k_{obs}(P - P_{eq})^2 \qquad (2)$$

where P_{eq} is the equilibrium pressure. No mechanism supporting this or any other rate law was presented. Furthermore, such a rate law is physically unacceptable because it breaks down for $P > P_{eq}$; that is, it predicts that the pressure would *increase* in time and thus not decrease to approach P_{eq} under these circumstances. One additional difficulty with this study is the poor correlation between ln k_{obs} and $1/T$, although Arrhenius behavior was observed for the *initial* rate of the reaction.

The question that we address in this study concerns the mechanism by which this unusual reversible reaction occurs. This problem is especially interesting because CA has been suggested as an intermediate in this process.[6,7] CA has been the focus of theoretical calculations,[8−10] but direct evidence of its existence does not appear to have been reported. To aid us in our search for the mechanism of the reversible dissociation

S1089-5639(98)00376-4 CCC: $15.00
Published on Web 05/08/1998

of AC, we performed high-level ab initio calculations of CA and examined its structure and potential energy surface with respect to both unimolecular and bimolecular decomposition pathways. We used the results of this study as a guide in determining the plausibility of various mechanisms, as we will discuss below.

In our experimental approach, we studied the kinetics of AC dissociation between 278 and 312 K in order to test mechanisms for this heterogeneous, reversible process. We therefore used a pressure transducer to follow the time dependence of the pressure above a thermostated sample of AC immediately after its rapid exposure to the constant, initially evacuated volume of an isoteniscope. The $t = 0$ boundary condition, i.e., the onset of the reaction is established by rapidly exposing the solid AC sample to an evacuated headspace. The subsequent pressure increase due to the formation of volatile reaction products was followed in real time using the pressure transducer.

We considered two generally different scenarios for the reversible decomposition of AC: a process involving the gas-phase species A, C, and CA and a solid-state mechanism in which the postulated CA intermediate does not leave the surface of AC. We will present indirect arguments in support of the solid-state mechanism.

Experimental Section

Ammonium carbamate (Aldrich) was used as received; it was stored in a cool, dry environment. The apparatus was an all-glass isoteniscope (total volume ca. 34 mL) having a bulb (3.0 cm diam) at the bottom. The isoteniscope was connected to a vacuum line via a 0.5-mm quick-opening PTFE stopcock. A stainless steel pressure transducer having a range of 0−15 psia (Omega Engineering PX176) was attached to the isoteniscope. The transducer was powered by a 15-V dc regulated power supply and has a specified response time of 20 ms (50 Hz). It was calibrated against a mercury Barometer; its null offset and ambient pressure voltages were measured between 0 and 50 °C. The output of the transducer was fed into an analog-to-digital converter (ADC) (Windaq DI-180, Dataq Instruments, Dayton, OH), which was interfaced through an RS232 communications port to a Windows 95-based PC. The isoteniscope, including the entire transducer apparatus, was immersed in a constant-temperature bath capable of 0.05 °C regulation. Bath temperatures were read using a calibrated thermometer.

Approximately 0.3 g of the solid was introduced to the bulb of the isoteniscope and was degassed via several pump−sublime cycles. To ensure maximal thermal contact between the ammonium carbamate and the bath, the solid was sublimed onto the inner surface of the isoteniscope bulb. The $P(t)$ data were acquired immediately after an initial evacuation of the headspace above the solid in the isoteniscope until the pressure leveled off (about 2 min for the lowest temperature run, 40 s for higher temperatures). A given sample of AC was subject to several evacuation cycles during the course of variable temperature experiments. The data density was 8 points per second in all runs. The Fourier transform infrared (FTIR) spectrum of the vapor in equilibrium with the solid ($T = 302$ K) was obtained at a resolution of 2 cm^{-1} in a 19.5-cm cell fitted with KBr windows using a Midac Instruments Model 2000. Spectra of CO_2 and NH_3 were acquired in a 10-cm cell under the same experimental conditions.

Data analyses were carried out using RS/1, a scientific and statistical spreadsheet (BBN Software Products, Cambridge, MA). Kinetic simulations were performed with KINETIC,[11] a kinetics simulation software package.

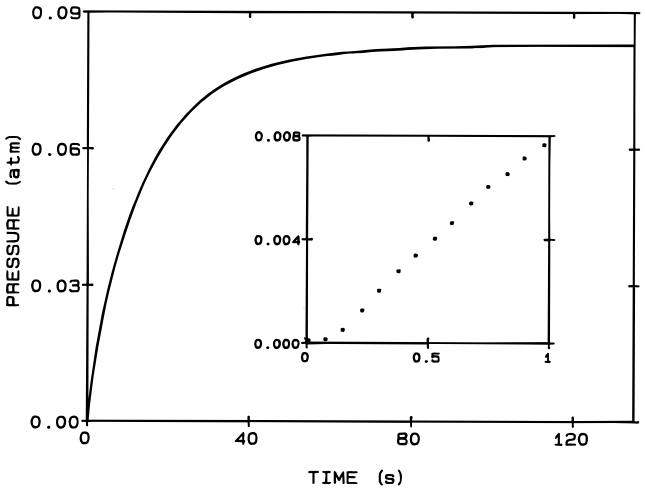

Figure 1. Time dependence of pressure over solid AC due to its decomposition into A and C at 293.7 K. Inset: The pressure change during the first second of the run, showing the inflection; each dot is a data point.

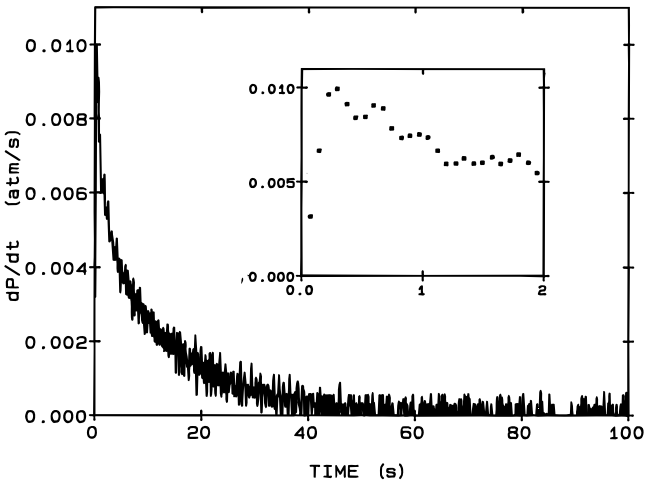

Figure 2. Plot of $\dot{P}$ vs t for the data shown in Figure 1. Inset: the first two seconds of the run, in which the maximum shows up more clearly.

Because the mechanisms that we tested all lead to various differential rate laws, which are expressions of $\dot{P}(P)$, where $\dot{P} = dP/dt$, we performed numerical differentiation of the raw $P(t)$ data to obtain $\dot{P}(t)$ arrays which were subsequently smoothed and transformed using a cubic spline technique[12] into $\dot{P}(P)$ arrays that were equispaced in P.

Results and Discussion

Given the good time resolution associated with the real-time $P(t)$ data, we were encouraged to seek a mechanism for the reversible dissociation process that was consistent with the experimental rate law as well as the temperature dependence of the equilibrium pressure (and thus the enthalpy of reaction). Figure 1 shows the data for the time dependence of the pressure over solid AC at 293.7 K. The inset in Figure 1 displays the $P(t)$ data for the first 1 s of the reaction. It can be noticed from the inset that there is an inflection in the data, which is enhanced by taking the derivative of the $P(t)$ data, i.e., $\dot{P}(t)$. This inflection property was highly reproducible, even after several evacuation cycles on a given sample (see the Experimental Section). Figure 2 displays $\dot{P}$ vs t obtained from the data shown in Figure 1. Here, the inflection in the $P(t)$ data is clearly revealed as a maximum. Figure 3 shows a plot of $\dot{P}$ vs P for the same run.

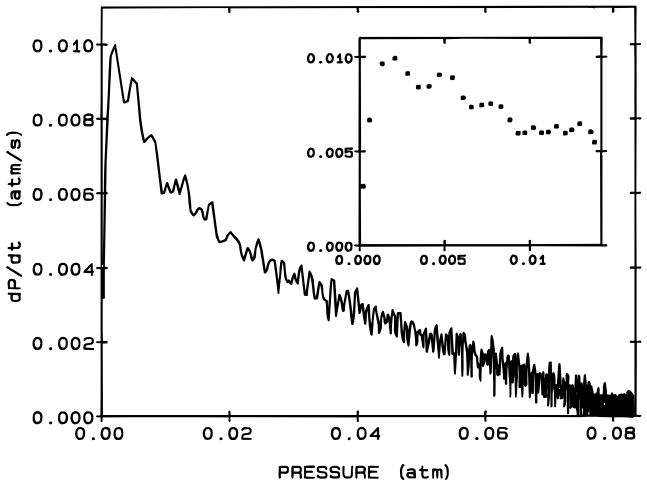

Figure 3. Plot of $\dot{P}$ vs P for the data shown in Figure 1. Inset: the first two seconds of the run, in which the maximum shows up more clearly.

Several important features of this plot need mentioning: (1) the plot is nonlinear; (2) like the $\dot{P}(t)$ curve, it also shows a maximum corresponding to the inflection in the $P(t)$ curve; (3) the magnitude of its derivative decreases after the maximum (i.e., the second derivative is positive), and (4) it intersects the P-axis at a finite pressure that corresponds to the equilibrium pressure P_{eq}. The $P(t)$ [as well as the $\dot{P}(t)$ and $\dot{P}(P)$] plots obtained at the other temperatures qualitatively resemble those shown in Figures 1 and 2. The presence of the inflection in the $P(t)$ curves likely implies that there is at least one sequential step in the mechanism by which the gas-phase species (i.e., A and/or C) are produced.[13]

We considered several mechanisms that explicitly involve gas-phase CA in the AC $\rightleftharpoons$ 2A + C reaction. Many of those were rejected because their rate laws failed to conform even to the shape of the curve shown in Figure 1 for all reasonable values of the relevant rate constants. We also evaluated several empirical differential rate laws. We discarded the "one-step" mechanism involving the expulsion of 2A + C from the AC surface and the termolecular reverse step because it predicts a rate law of the form $\dot{P} = a - bP^3$, which is not compatible with the observed rate data. Furthermore, our data are also incompatible with empirical first-, second-, and third-order rate laws, i.e., $\dot{P} = k(P_{eq} - P)$, $\dot{P} = k(P_{eq} - P)^2$, and $\dot{P} = k(P_{eq} - P)^3$, respectively.

Mechanisms

We will begin by discussing two mechanisms that yield rate laws that conform qualitatively to the experimental $P(t)$, $\dot{P}(t)$, and $\dot{P}(P)$ data. Mechanism 1 contains three reversible steps

Mechanism 1.

$$\mathrm{AC}' \underset{k_{-1}}{\overset{k_1}{\rightleftharpoons}} \mathrm{CA} + \mathrm{A}$$

$$\mathrm{CA} \underset{k_{-2}}{\overset{k_2}{\rightleftharpoons}} \mathrm{X} \qquad (3)$$

$$\mathrm{X} \underset{k_{-3}}{\overset{k_3}{\rightleftharpoons}} \mathrm{A} + \mathrm{C}$$

and accounts for the reversibility of the process. AC′ symbolizes the ammonium carbamate formula unit as a solid-state species, which exists on the surface of the AC sample; all other entities are present in the gas phase. X represents a loose van der Waals complex formed between ammonia and carbon dioxide. The inclusion of this species avoids the necessity for assuming specific orientational requirements for the collisions between A and C to form CA. According to this mechanism, proton transfer from the ammonium ion to the carbamate ion forms carbamic acid and ammonia, which are then expelled from the surface into the gas phase. Carbamic acid then undergoes unimolecular isomerization to form the more loosely bound species, X, which itself then dissociates into NH_3 and CO_2. Furthermore, the forward reaction in the first step, i.e., AC′ $\rightarrow$ CA + A, is assumed to be a pseudo-zero-order process; thus the rate constant k_1 is treated as an *extensive* quantity, i.e., $k_1 = k_1'S$, where S is the effective surface area of the solid AC sample, which is assumed to be constant on the time scale of the experiment (ca. 40 s at higher temperatures and 2 min at the lowest one), and k_1' is the true first-order rate constant. It is implicit in eqs 3 that k_{-1} is also extensive in order that the equilibrium constant expressed by k_1 to k_{-3} be intensive.

It is evident from mechanism 1 that C is formed sequentially (step 3), while A is produced both initially (step 1) and sequentially (step 3) after the onset of the reaction. The complex X is also formed sequentially (step 2), but its concentration is presumed to be very low (see below). Thus it would seem that this mechanism might be compatible with the early-time inflection observed in the $P(t)$ data. Indeed, we were able to simulate reaction profiles that closely resembled the data depicted in Figures 1 and 2.[11] However, we did not perform a global regression analysis on the data with respect to the six rate constants contained in mechanism 1 because we were unable to obtain $P(t)$ analytically from the set of four coupled differential equations that this mechanism generates.

To estimate these rate constants (and also to obtain the equilibrium constant analytically), we invoked the steady-state approximation for the intermediates CA and X with the result that for times after the build-up of CA and X, $\dot{P}(P)$ is given by

$$\dot{P}(P) = \frac{a - bP^3}{1 + cP} \qquad (4)$$

where

$$a = 3k_1$$

$$b = \frac{4k_{-1}k_{-2}k_{-3}}{9k_2k_3} \qquad (5)$$

and

$$c = \frac{2k_{-1}(k_3 + k_{-2})}{3k_2k_3}$$

We carried out a regression analysis on the postinflection part of the splined $\dot{P}(P)$ data (e.g., $>8.5 \times 10^{-4}$ M for the 293.7 K run) using eq 4. In this analysis, the rate constants and the parameters a, b, and c have been converted to molarity units even though pressure units are implicit in eq 2. From our regression analysis of the data at 293.7 K, we obtained $a = 4.03 \times 10^{-4}$ ($\sigma = 1 \times 10^{-6}$), $b = 10\,230$ ($\sigma = 33$), and $c = 1211$ ($\sigma = 7$). According to eq 4, $K_c = 4a/27b$, and this expression was used to obtain K_c at the different temperatures studied. These equilibrium results are discussed later.

To simulate[11] the $P(t)$, $\dot{P}(t)$, and $\dot{P}(P)$ curves shown in Figures 1−3, the values of the six rate constants, k_1 to k_{-3}, were so chosen as to conform both to the values of a, b, and c obtained in the regression (expressions in eq 5) and also to the value of

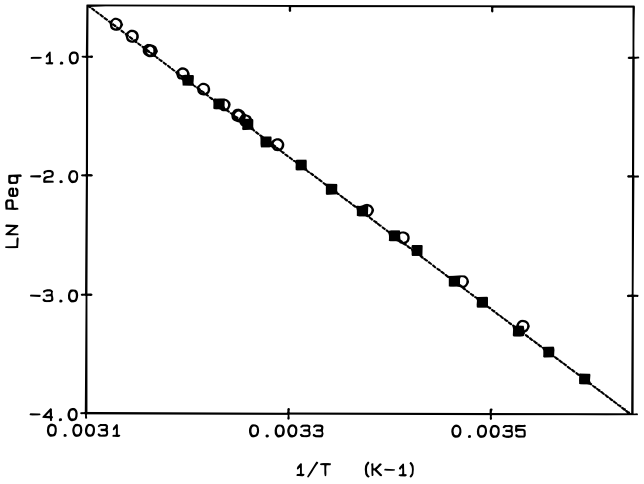

Figure 4. Van't Hoff plot of P_{eq} for the decomposition of AC: (◆) our results; (⊙) literature data; (- - -) linear regression fit to our values [slope = −6373 (σ = 24) K; intercept = 19.20 (σ = 0.08].

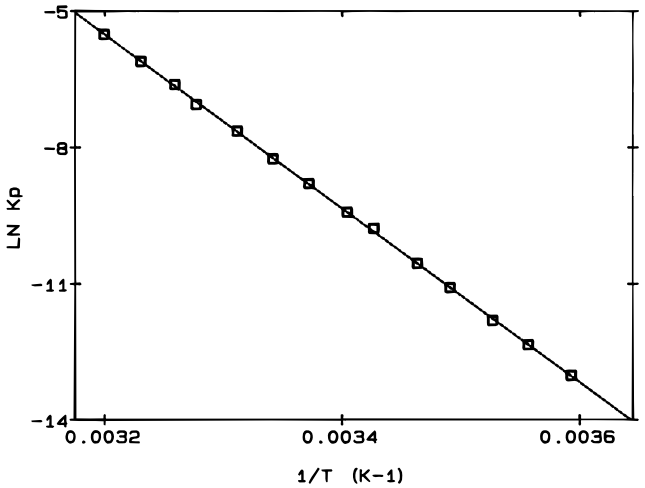

Figure 5. Van't Hoff plot of K_P for the AC decomposition: (◇) our results; (- - -) linear regression fit [slope = −19,120 (σ = 72) K; intercept = 55.70 (σ = 0.24)].

the equilibrium constant, K_c, i.e., $k_1k_2k_3/k_1k_{-2}k_{-3}$. (The rate constants used in the simulation were $k_1 = 1.29 \times 10^{-4}$ s^{-1}, $k_{-1} = 1.10 \times 10^4$ M^{-1}s^{-1}, $k_2 = 14.0$ s^{-1}, $k_{-2} = 1.40 \times 10^2$ s^{-1}, $k_3 = 1.20 \times 10^2$ s^{-1}, and $k_{-3} = 24.3$ M^{-1}s^{-1}.) Those simulated curves closely match the experimental curves shown in Figures 1−3.

With the exception of k_1, which is equal to a/3, the other rate constants cannot be obtained uniquely because the set of three equations with six unknown rate constants, eq 5, is underdetermined. An Arrhenius plot of k_1 between 278.3 and 316.0 K was linear with an activation energy of 11.47 (σ = 0.43) kcal/mol. The Arrhenius plots for parameters b and c are also linear, but with *positive* slopes of 24.76 (σ = 0.37) kcal/mol and 2.78 (σ = 0.08) kcal/mol, respectively. To confirm the extensive nature of k_1, we obtained a series of $\dot{P}(P)$ data with varying amounts of solid AC placed in the isoteniscope chamber at 297.3 K. In these experiments, the AC samples were not sublimed onto the inner surface. A double logarithmic plot of k_1 vs AC sample mass was found to be linear with a slope of 0.87 (σ = 0.09), indicating the extensive nature of k_1 which is consistent with a pseudo-zero-order process. A double logarithmic plot of the parameter b was also linear (slope = 0.88, σ = 0.15); we believe that the extensive nature of b arises mainly from the extensive nature of k_{-1} (see eq 5).

The Equilibrium State

When the AC−A−C system attains equilibrium, $P = P_{eq}$ and $\dot{P} = 0$, and hence, P_{eq} can be expressed analytically in terms of parameters a and b by setting the right-hand side of eq 4 to zero and solving for P_{eq} as shown in eq 6.

$$P_{eq} = \left(\frac{a}{b}\right)^{1/3} \tag{6}$$

Figure 4 shows a van't Hoff plot of the P_{eq} data obtained thus from our experiments. The plot is linear with a slope of 12.66 (σ = 0.05) kcal/mol. In Figure 4 we have also included for comparison several P_{eq} values that have been reported previously.[1,2] As can be seen from this comparison, our results are in excellent agreement with the literature values.

The overall equilibrium constants K_c and K_P of the AC ⇌ 2A + C reaction can be obtained using the following relations

$$K_P = \frac{4}{27}P_{eq}^{\ 3} = \frac{4a}{27b} \quad \text{and} \quad K_P = K_c(RT)^3 \tag{7}$$

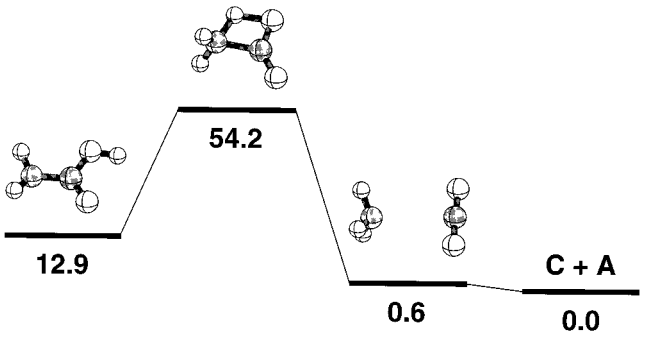

Figure 6. Free energy profile for the gas-phase decomposition of CA to yield products A and C (see mechanism 1). Free energies (MP2/6-31+G*) are given in kcal/mol relative to those of the infinitely separated products.

K_c is equal to $k_1k_2k_3/k_{-1}k_{-2}k_{-3}$, [i.e., $K_{c1}K_{c2}K_{c3}$, where K_{c1}, K_{c2}, and K_{c3} are the equilibrium constants of the three consecutive, elementary kinetic steps represented in mechanism 1 (eqs 5 and 7)]. This expression is consistent with that mechanism. Figure 5 shows a van't Hoff plot of K_P values, from which ΔH = 37.99 (σ = 0.14) kcal/mol is obtained. This value is in very good agreement with ΔH of 38.19 kcal/mol, calculated from the $\Delta H_f°$ data for AC, C, and A,[14] and also with previously reported values, i.e., 37.6 kcal/mol[2] and 38.8 kcal/mol.[3]

Ab Initio Calculations

To obtain additional insight into the AC decomposition mechanism, particularly the second and third steps of mechanism 1, we calculated the free energy profile for the decomposition of CA using high-level ab initio methods. Equilibrium and transition state geometries were fully optimized at the MP2 level of theory using the standard 6-31+G* basis sets. Each geometry was characterized by calculating harmonic vibrational frequencies, and free energies (at 298 K) were evaluated using standard statistical mechanics formulas.[15] All calculations were performed with the Gaussian 94 package.[16] Raw MP2 energies and optimized structures (in Gaussian format) are available in the Supporting Information.

The most significant outcome of these calculations, as they pertain to mechanism 1, is that the gas-phase CA molecule is remarkably stable with respect to the unimolecular decomposition. Figure 6 shows the calculated free energy profile for the decomposition of CA. CA reacts via the in-plane transfer of

the OH proton to the amino group, resulting in the scission of the CN bond to give A and C. Relative to the separated A and C products, CA has a free energy of 12.9 kcal/mol. The free energy of the transition state is significantly larger, 54.2 kcal/mol, corresponding to a considerable barrier to decomposition of 41.4 kcal/mol. Despite a positive entropy of activation, the rate constant for CA → A + C is clearly much too small ($k \approx 10^{-18}$ s^{-1}) to be of kinetic importance at the temperatures studied here. Even allowing for some uncertainty in the magnitude of reaction barrier to the decomposition of AC, we regard these computational results as being sufficiently reliable to cast very serious doubt as to the validity of mechanism 1.

The thermodynamic stability of CA has been previously calculated by Wen and Brooker[9] at the SCF level and by Remko and co-workers[8,10] at higher levels of theory (MP2 to MP4). These calculations generally reveal that CA is either isoenergetic with or slightly more stable than the separated products A and C.[17] Zero-point energy (ZPE) corrections tend to destabilize CA relative to A + C. Thus, at the MP4/6-31G**+ZPE level, Remko and Rode[10] report that the decomposition of CA is exothermic (at 0 K) by −6.2 kcal/mol. This result compares favorably with our MP2/6-31+G*+ZPE value of −4.2 kcal/mol, which, after applying temperature and entropic corrections, yields the −12.9 kcal/mol exergonicity of Figure 6.

Due to the predicted kinetic stability of gas-phase CA, and hence its inability to be directly converted to products as indicated in mechanism 1, we were led to consider an alternative process for the decomposition of CA, namely, the bimolecular ammonia-assisted process, CA + A → X + A.

Mechansim 2.

$$\begin{aligned} \mathrm{AC}' &\underset{k_{-1}}{\overset{k_1}{\rightleftharpoons}} \mathrm{CA} + \mathrm{A} \\ \mathrm{CA} + \mathrm{A} &\underset{k_{-2}}{\overset{k_2}{\rightleftharpoons}} \mathrm{X} + \mathrm{A} \\ \mathrm{X} &\underset{k_{-3}}{\overset{k_3}{\rightleftharpoons}} \mathrm{A} + \mathrm{C} \end{aligned} \tag{8}$$

where both k_2 and k_{-2} are now second-order rate constants. Like mechanism 1, mechanism 2 is also fundamentally plausible because it involves the presence of sequentially formed species and, accordingly, predicts an inflection in the $P(t)$ profile. Thus, it is possible to simulate reasonable representations of the $P(t)$ data, but as stated earlier, we cannot perform global regression on the data. Application of the steady-state approximation to the intermediate species, CA and X, in mechanism 2 leads to a rate law that is identical in functional form to that of mechanism 1 (eq 4), although the parameters *a*, *b*, and *c* are now functions of the rate constants k_1 through k_{-3} that are different from those shown in eq 5. Thus mechanisms 1 and 2 are indistinguishable by regression analysis alone.

Because both mechanisms 1 and 2 require the presence of gas-phase carbamic acid, we sought direct evidence for the existence of this species. Accordingly, we examined the FTIR spectrum of the headspace vapor in equilibrium with solid CA at 303 K using a 20-cm path length cell. The ab initio calculations suggest that the strongly allowed CO stretching frequency of CA lies at 1982 cm^{-1}, which is in a region that is unencumbered by absorption by both NH_3 and CO_2. We carefully examined the region between 1850 and 2200 cm^{-1} but were unable to observe any features that could be assigned to the CA carbonyl stretch. In their study of the Raman spectra of aqueous solutions of ammonium carbamate, Wen and Brooker found no evidence of the presence of molecular carbamic acid.[9]

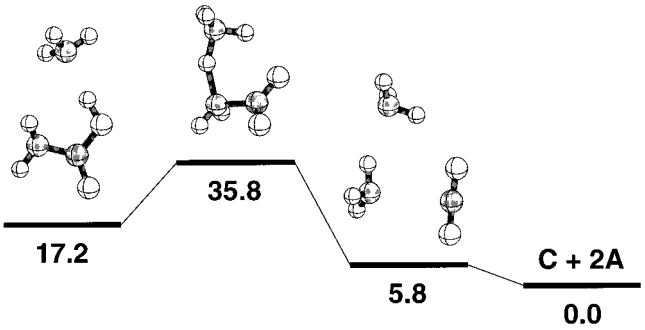

Figure 7. Free energy profile for the ammonia-assisted decomposition of CA to yield products A and C (see mechanism 2). Free energies (MP2/6-31+G*) are given in kcal/mol relative to those of the infinitely separated products.

This is not surprising in view of the expectation that carbamic acid would rapidly and effectively undergo hydrolysis in this environment.

We also sought evidence of the van der Waals complex, X (see eqs 4 and 8), by examining the rovibrational features of the out-of-plane bending mode of NH_3 in the 750−1250 cm^{-1} region. In a comparison of the spectrum of NH_3 in equilibrium with AC with that of NH_3 itself, we found no evidence to suggest the presence of additional, shifted features that would be expected for the complex. Thus, our failure to find definitive evidence from the IR spectra for the existence of CA or for the van der Waals complex does not allow mechanism 2 to be proposed definitively, at least in the absence of other supporting data. It is important to point out that, according to mechanisms 1 and 2, the steady state concentration of CA is expected to be very low, and thus, our failure to find direct IR evidence for this species does not necessarily rule out their existence.

In view of our rejection of mechanism 1 on the basis of the computational results presented above, we also explored mechanism 2 by performing ab initio calculations to determine whether the high stability found for CA would be lower for the bimolecular decomposition step. Figure 7 shows the calculated free energy profile for this reaction. This process is clearly less strongly activated than the unimolecular reaction, having a free energy of activation, 18.9 kcal/mol, which is significantly lower than that of the second step of mechanism 1. The reaction coordinate involves a double proton transfer, first from OH to the assisting ammonia molecule to form an ammonium cation and second from ammonium to the amino group. The second transfer simultaneously cleaves the CN bond of carbamate yielding a van der Waals complex of two A molecules with C. Bimolecular decomposition of CA is considerably more plausible than the unimolecular decomposition step of mechanism 1.

Although the surface reaction of mechanism 2 (step 1) cannot be directly examined by calculation, its endothermicity can be judged from the enthalpy changes calculated for steps 2 and 3 and the overall endothermicity of the AC decomposition (38.0 kcal/mol, Figure 5). The calculations suggest that the latter two steps of mechanism 2 are exothermic by 3.5 kcal/mol. Thus, the surface reaction must be endothermic by roughly 41.5 kcal/mol. This value is, however, inconsistent with the 11.5 kcal/mol activation energy obtained from the Arrhenius plot of k_1. As with mechanism 1, our calculations lead us to abandon mechanism 2.

Another difficulty with Mechanisms 1 and 2 is that in the back reaction, solid AC must be produced through a bimolecular collision between CA and A, which, in view of the apparent low number density of CA, must correspond to a very low

probability event. Our attempts to model other mechanisms that contained single-molecule collisions with the AC surface to represent the back reaction were unsuccessful because the rate laws obtained predicted $\dot{P}(t)$ curves that are inconsistent with the observed data.

Mechanism 3. In this mechanism, the reaction steps leading to the formation of the small molecules A and C from solid AC are assumed to take place *on its surface*; i.e., A and C are the only gas-phase species present.

$$\begin{aligned} \mathrm{AC}' &\underset{k_{-1}}{\overset{k_1}{\rightleftharpoons}} \mathrm{CA}' + \mathrm{A}' \\ \mathrm{CA}' &\underset{k_{-2}}{\overset{k_2}{\rightleftharpoons}} \mathrm{A}' + \mathrm{C}' \\ \mathrm{A}' &\underset{k_{-3}}{\overset{k_3}{\rightleftharpoons}} \mathrm{A} \\ \mathrm{C}' &\underset{k_{-4}}{\overset{k_4}{\rightleftharpoons}} \mathrm{C} \end{aligned} \qquad (9)$$

where the primed species represent surface-bound molecules. This mechanism contains eight rate constants. Furthermore, it shows that the dissociation of CA′ is a first-order process. In view of the ab initio calculations supporting the stability of CA, this process is nevertheless reasonable because it is likely to be assisted by neighboring ammonium ions on the solid surface/matrix.

In this context, it is useful to consider the solid-state structure of AC. Gieren et al.[18] and Adams et al.[19] have reported the following structural data for solid AC based on X-ray crystallographic studies. The NH_2COO^- ions (denoted hereafter as CA^-) form head-to-head, roughly planar, centrosymmetric dimers that are arranged in parallel layers. The NH_4^+ ions (denoted hereafter as A^+) form interpenetrating double layers that are sandwiched between the anion layers. Each A^+ ion is hydrogen-bonded through its H-atoms to the O-atoms of four separate CA^- ions (three on one side and one on the other) and each O atom of the CA^- anion is hydrogen bonded to two A^+ ions. The A^+ ions thus cross-link the anion layers, as well as the anions within each layer. The N−H···O hydrogen bond distances range from 1.77 and 2.19 Å.

Although the surface structure of solid AC may not exactly correspond to its interior structure as described in the previous paragraph, it is reasonable to assume that the dimeric anions hydrogen-bonded to the ammonium ions do exist on the surface. Thus a surface (and maybe bulk) reaction leading to the reversible decomposition of AC′ into A′ and C′ may be quite facile. Such a scheme is portrayed schematically in Figure 8, which represents the solid/surface structure of AC.

Mechanism 3 is reasonably compatible with this solid-state structure of AC. The H atom of an A^+ ion, which is already hydrogen-bonded to the O-atom of an AC^- ion, can readily undergo a transfer (as H^+) to the anion, leading to the formation of carbamic acid (CA′) and ammonia (A′) on the surface (or within the matrix) of AC. The CA′ species, assisted by the other CA^- unit of the dimer, can then undergo decomposition into C′ and a second A′ molecule. Such a scheme may also be used to account for the reverse process, i.e., the formation of solid AC from gaseous A and C. Successive adsorption onto a surface, such as glass, of alternate layers of A and X (the van der Waals complex of A and C) can lead to the formation of CA′ via hydrogen bonding and proton transfer. This CA′ species can then react with A′ to produce AC.

On the basis of infrared studies of AC formation from gaseous A and C that had been adsorbed on a surface at low temperature,

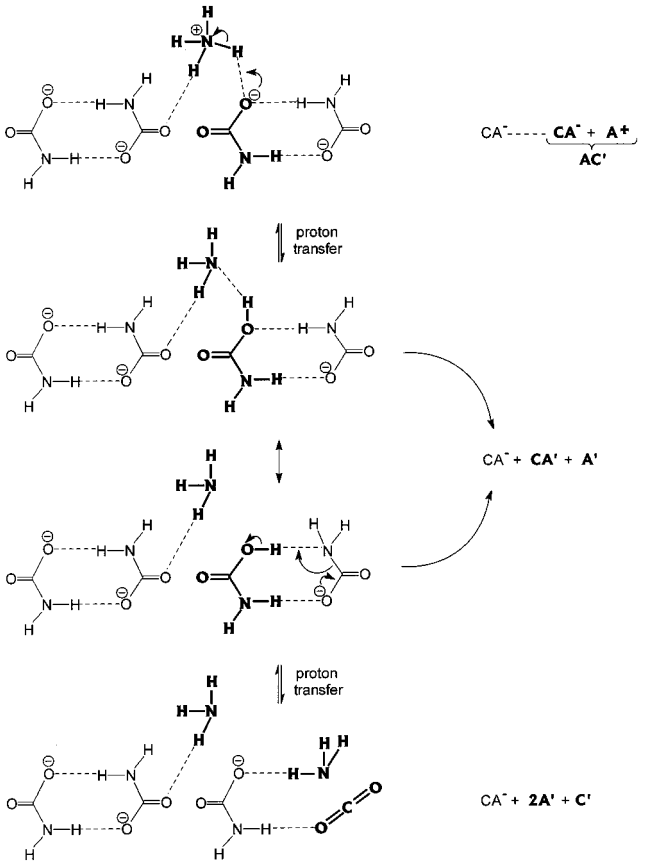

Figure 8. An illustration of the solid state/surface processes (steps 1 and 2) occurring in the solid state mechanism (mechanism 3) for the decomposition of AC. Two anionic dimers and one ammonium ion are shown. The species that are involved in the net process are shown in boldface. The nearby ions merely assist the process.

Hisatsuni has suggested that crystalline AC may be formed from an unstable precursor consisting of a 2:1 complex between A and C in which the NH_3 molecules are not equivalent.[20] It thus seems possible that such a species, i.e., $(NH_3)_2CO_2$, is involved as an intermediate in the decomposition of solid AC. Mechanism 3 is indeed consistent with this idea (see Figure 8).

We note that although the AC^- anion-assisted decomposition of CA′ may be viewed a second-order process, the *local* concentration of the neighboring AC^- ions can be assumed to be a constant. Thus, the dissociation of CA′ in mechanism 3 can be represented as a pseudo-first-order process.

With reference to eqs 9, we use the following approximations to simplify the kinetic treatment of this mechanism: (a) $k_3 \approx k_4 \equiv k_d$ and $k_{-3} \approx k_{-4} \equiv k_a$, and (b) $[\mathrm{CA}'] \ll [\mathrm{A}'], [\mathrm{C}']$, i.e., $[\mathrm{A}'] \simeq 2\,[\mathrm{C}']$, where [CA′], [A′], and [C′] are the time-dependent surface concentrations of CA, A, and C, respectively. Thus, the following differential rate law is obtained:

$$\dot{P} = k_d([\mathrm{A}'] + [\mathrm{C}']) - k_a P \simeq 3k_d[\mathrm{C}'] - k_a P \qquad (10)$$

Because of the complexity of the system of coupled differential equations that pertains to the kinetics of mechanism 3, we are not able to express $\dot{P}(P)$ [or $P(t)$] analytically and, therefore, did not carry out a global analysis of the kinetic data.

From the details given in the Experimental Section, it is reasonable to assume that prior to evacuation and data acquisition, the solid AC is in equilibrium with the surface-bound species A′, C′, and CA′ as well as with the gas-phase species A and C, as depicted by the equilibrium steps in eqs 9. The concentrations of the species involved can then be expressed

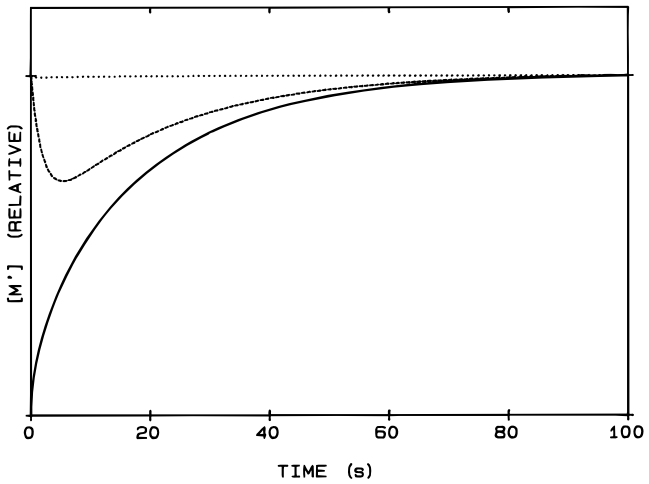

Figure 9. A qualitative diagram showing the time dependence of the concentration of the surface-bound species A′ and C′ in mechanism 3 under various kinetic scenarios: (•••) *case 1, subcase a* ($k_1 = 31.3$; $k_{-1} = 3.0 \times 10^7$; $k_2 = 51.3$; $k_{-2} = 55.5$; $k_d = 0.012$; $k_a = 0.066$); (- - -) *case 1, subcase b* ($k_1 = 9.5 \times 10^{-4}$; $k_{-1} = 1.48 \times 10^5$; $k_2 = 20.0$; $k_{-2} = 11.0$; $k_d = 0.19$; $k_a = 0.24$); (—) *case 2* ($k_1 = 2.85 \times 10^{-3}$; $k_{-1} = 4.59 \times 10^5$; $k_2 = 60$; $k_{-2} = 4.13$; $k_d = 0.6$; $k_a = 1.5$). Here the surface-bound species are collectively shown as M′. These plots are based on our kinetic simulations with assumed rate constants.

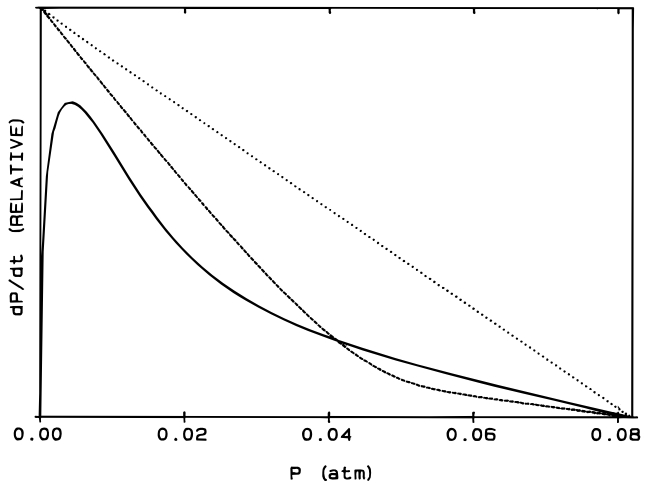

Figure 10. A qualitative diagram showing the $\dot{P}(P)$ plots obtained for mechanism 3 under various kinetic scenarios: (•••) *case 1, subcase a*; (- - -) *case 1, subcase b*; (—) *Case 2*. These plots are based on the same simulations portrayed in Figure 9.

as $[A'] = [A']_{eq}$; $[C'] = [C']_{eq}$; $[CA'] = [CA']_{eq}$; $[A] = [A]_{eq}$; and $[C] = [C]_{eq}$, where the subscript "eq" stands for equilibrium conditions. The solid is suddenly exposed to an evacuated headspace. The question arises as to the effect of evacuation on the concentrations of surface-bound species A′, C′, and CA′ and their approach to equilibrium. Two limiting scenarios can be envisaged for this process (see eqs 9).

Case 1: Here we assume that evacuation of the headspace removes *only* the gas-phase molecules A and C (and, hence, *does not* deplete the surface-bound species A′, C′, and CA′). At this juncture, we consider two subcases. In subcase a, desorption of A′ and C′ to form A and C, respectively, occurs relatively slowly as compared with the first two steps in eq 9, and the surface concentrations of A′ and C′ are never altered during the reaction and, thus, are established by their equilibrium concentration values. In this situation, the differential rate law (eq 10) becomes

$$\dot{P} = k_d([A']_{eq} + [C']_{eq}) - k_a P \simeq 3k_d[C']_{eq} - k_a P \quad (11)$$

Equation 11 predicts that $\dot{P}(P)$ is linear in P and, thus, is inconsistent with our experimental results. We could mimic this situation in our simulations and illustrate it qualitatively in Figures 9 and 10. The rate constants used are listed in the caption. These rate constants are chosen such that the K_c values are identical in each simulation and are equal to the experimental value at ca. 294 K, i.e., 5.8×10^{-9}. In subcase b, desorption of A′ and C′ occurs more rapidly, and eq 10 describes the rate of formation of gas-phase A and C in which [A′] and [C′] would begin at their equilibrium values, $[A']_{eq}$ and $[C']_{eq}$, then go through a minimum due to depletion at early stages of the reaction, followed by a build-up at later stages, and again approach their equilibrium values (see Figure 9). In subcase b, the magnitude of the slope of $\dot{P}(P)$ versus P would decrease with increasing P, but this rate law *does not* predict the inflection that is observed in the experimental $P(t)$ curve [i.e., the maxima in the $\dot{P}(t)$ and $\dot{P}(P)$ curves]. This behavior, which is also illustrated in Figure 10, is inconsistent with our experimental results.

Case 2: Here we assume that the initial evacuation of the headspace above the solid AC not only depletes the gas-phase A and C but also *completely* removes the surface-bound species A′, C′, and CA′. The time dependence of the surface-bound species is illustrated in Figure 9. Under these conditions the $\dot{P}(t)$ and $\dot{P}(P)$ curves would show maxima, corresponding to an inflection in the $P(t)$ curve. This scenario is also consistent with the increase in the magnitude of the slope that is observed in the $\dot{P}$ versus P curve (Figure 10).

The actual kinetic behavior of the AC decomposition may correspond to an intermediate situation between the above limiting cases. Our simulations[11] indicate that the inflection would be observable if the initial depletion of the surface-bound small molecules is at least 65%, i.e., the initial concentrations of the surface-bound molecules are not more than 35% of their equilibrium concentrations.

Conclusion

Each of the three detailed mechanisms proposed for the reversible decomposition of ammonium carbamate is consistent with the inflection seen in the experimental kinetic data. However, the first two "gas phase" mechanisms are incompatible with the ab initio calculations, indicating that the carbamic acid intermediate postulated in these mechanisms is too stable to play the transient role that is required. Thus we cast aside these "gas phase" mechanisms because we consider the calculations reliable enough, especially in view of the considerable stability that is associated with carbamic acid and of our failure to observe this species spectroscopically.

The third or "solid-state" mechanism that we propose seems most plausible. First, it does not require the presence of carbamic acid in the gas phase. Second, it is reasonable in the context of the known solid state structure of carbamic acid. And third, it is qualitatively consistent with kinetic simulations based on reasonable values of the rate constants. Further studies dealing with species-specific kinetics will be pursued to substantiate this mechanism and, it is hoped, allow a more quantitative determination of the rate constants to be made.

Supporting Information Available: Optimized geometries and energies for the structures shown in Figures 6 and 7 available in the form of Gaussian input decks (3 pages). Ordering information is given on any current masthead page.

References and Notes

(1) Laurent, V.; Kikindai, T. *Bull. Soc. Chim. Fr.* **1972**, 1258.
(2) Briggs, T. R.; Migrdichian, V. *J. Phys. Chem.* **1924**, *28*, 1121.
(3) Egan, E. P., Jr.; Potts, J. E., Jr.; Potts, G. D. *Ind. Eng. Chem*. **1946**, *38*, 454.
(4) Janjic, D. *Helv. Chim. Acta* **1964**, *47*, 1879.
(5) Frejacques, M. *Chim. Ind*. **1948**, *68*, 22.
(6) Lishnevskii, V. A.; Madzievskaya, T. A. *Russ. J. Phys. Chem*. **1982**, *56*, 1342.
(7) Claudel, B.; Boulamri, L. *Thermochim. Acta* **1988**, *126*, 129.
(8) Remko, M.; Scheiner, S. *J. Mol. Struct. (THEOCHEM)* **1990**, *204*, 331.
(9) Wen, N.; Brooker, M. H. *J. Phys. Chem*. **1995**, *99*, 359.
(10) Remko, M.; Rode, B. M. *J. Mol. Struct. (THEOCHEM)* **1995**, *339*, 125.
(11) KINETIC, Version 3.11, Milescu, L., Bucharest, Romania; (lorin@cbb.bth.ro).
(12) Press: W. H.; Flannery, B. P.; Teukolsky, S. A.; Vetterling, W. T., *Numerical Recipes*; Cambridge University Press: New York, 1986; pp 86−89.
(13) We considered the possibility that the inflection in the $P(t)$ curves was caused by the cooling of the solid AC sample as a result of evacuating the headspace in the isoteniscope and the subsequent warming of the sample during the early part of the equilibration process. We were unable to confirm this effect and, thus, are led to assume that the inflection feature is intrinsic to the AC decomposition kinetics.
(14) *Handbook of Chemistry and Physics*; 71st ed.; Lide, D. R., Ed.; CRC Press: Boca Raton, Fla., 1990; Vol. 25, p 43.
(15) Hehre, W. J.; Radom, L.; Schleyer, P. v. R., Pople, J. A. *Ab Initio Molecular Orbital Theory*; Wiley: New York, 1986.
(16) Frisch, M. J.; Trucks, G. W.; Schlegel, H. B.; Gill, P. M. W.; Johnson, B. G.; Robb, M. A.; Cheeseman, J. R.; Keith, T.; Petersson, G. A.; Montgomery, J. A.; Raghavachari, K.; Al-Laham, M. A.; Zakrzewski, V. G.; Ortiz, J. V.; Foresman, J. B.; Cioslowski, J.; Stefanov, B. B.; Nanayakkara, A.; Challacombe, M.; Peng, C. Y.; Ayala, P. Y.; Chen, W.; Wong, M. W.; Andres, J. L.; Replogle, E. S.; Gomperts, R.; Martin, R. L.; Fox, D. J.; Binkley, J. S.; Defrees, D. J.; Baker, J.; Stewart, J. P.; Head-Gordon, M.; Gonzalez, C.; Pople, J. A. *Gaussian 94, Revision C.3*; Gaussian, Inc.: Pittsburgh, PA, 1995.
(17) Remko and Scheiner,[8] however, reported MP2 and MP3/6-31G* calculations suggesting that CA is highly unstable, nearly 200 kcal/mol less stable than the products! This finding is inconsistent with all other reported calculations, even the more recent work of Remko and Rode,[10] who failed to comment on the source of the discrepancy in their calculations.
(18) Gieren, A.; Hoppe, W.; Fleischmann, K. *Angew. Chem., Int. Ed.Engl.* **1973**, *12*, 322.
(19) Adams, J. M.; Small, R. W. H. *Acta Crystallogr*. **1973**, *B29*, 2317.
(20) Hisatsune, I. C., *Can. J. Chem.* **1984**, *62*, 945.